Numerical analysis of the broadband interferometric sensor in a planar gradient-step index configuration

Marek Błahut

Department of Optoelectronics, Silesian University of Technology, Akademicka 2A, 44-100 Gliwice

Received April 25, 2022; accepted June 19, 2022; published June 30, 2022

Abstract—The paper presents the model of an optical sensor based on a two-mode interference in a planar gradient-step index configuration. The analyzed structure consists of a single-mode gradient index waveguide, made by Ag+-Na+ ion exchange, which is partially covered by a step-index SU-8 polymer layer. This step and gradient index structure forms a two-mode waveguide that is excited by a broadband light source from a selected spectral range. The refractive index variation of measured external surrounding affects the modal properties of a multimode waveguide and the spectral field distribution at the output of the structure.

The interference of modes in multimode waveguides depends on their propagation constants difference, which can be changed by the variations of light propagation conditions. This effect can be used in integrated interferometric sensors. One of the most straightforward configurations uses the interference of modes in a two-mode planar step-index optical waveguide [1].

A novel two-mode interferometric optical sensor in planar configuration proposed in this work is based on silver-sodium ion exchange in glass.

Glass integrated optical components made by ion exchange are developed today. Silver-sodium ion exchange is the most popular method for producing glass integrated optical components.

The essential part of the analyzed optical structure is a single-mode gradient index waveguide, partially covered, in the central part, by a step-index SU-8 polymer layer. It transforms the structure into a two-mode waveguide, where interference effects can be observed. The fabrication process of the analyzed configuration is cheap, fast, and easy technologically [2].

The sensor is designed to operate with a broadband light source. Its optical configuration is adjusted to examine biological solutions.

The configuration of the planar interference sensor is shown in Fig. 1. The structure consists of a gradient-index waveguide made by Ag+-Na+ ion exchange, forming the single-mode input and output. The gradient-index waveguide is covered in the central part by a step-index SU-8 polymer layer. This step and gradient index structure creates a two-mode waveguide where interference effects can be observed. The structure is excited by a broadband light source from a range of 0.55÷0.80μm, and the direction of light propagation is along the *z*-axis. The dispersion characteristic of a SU-8 polymer was determined in [3]. It is assumed that the optical system will be used to analyze biological substances. For that reason, the refractive index changes of the cover refer to the water solutions and can be expressed as $n_{H_2O} + \Delta n_c$ with Δn_c= (0÷0.005).

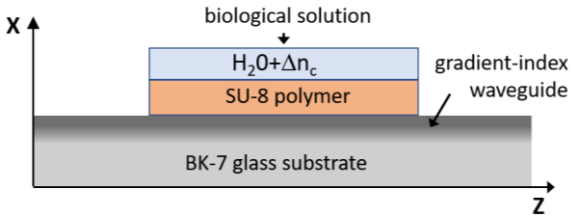

Fig. 1. Configuration of the sensor structure.

The refractive index variation of measured external surroundings affects the modal properties of the multimode waveguide. The image variations and spectral distribution are registered at the output of the single-mode waveguide.

Gradient index profile is the solution of a non-linear diffusion equation in BK-7 glass:

$$\frac{\partial C}{\partial t} = \nabla\left[\frac{D}{1-(1-m)\cdot C}\nabla C\right], \tag{1}$$

where C is the concentration of introduced Ag+ ions, proportional to the refractive index changes Δn, m is the mobility ratio of exchanged ions, and D is the diffusion coefficient.

It can be stated on the basis of experimental results [4], that Δn=0.1 near the surface of BK-7 glass and m=0.5. The dispersion characteristics of BK-7 glass are taken from [5]. The assumed diffusion depth $d_D = 4 \cdot \sqrt{D \cdot t_D}$ changes from 0.96mm to 1.31mm. The gradient-step index section is single mode for this geometry in the whole range of the examined wavelength.

The thickness w of the step index SU-8 polymer layer changes from 0.7mm to 0.9mm and its length L along the propagation direction amounts to 5000mm.

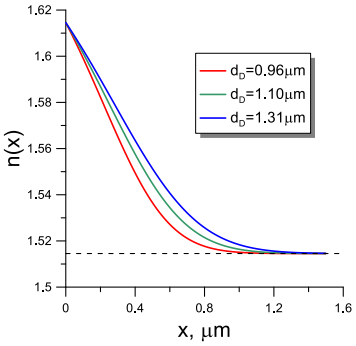

Fig. 2. Refractive index distribution $n(x)$ of gradient index waveguide for different diffusion times at the wavelength λ=0.65μm.

The operation principle of examined optical structure can be determined by modal field analysis [6].

The normalized wave function $\phi_{grd}(x)$ of the single-mode gradient index waveguide defines the field at the input of the two-mode step-gradient index section. This field is next decomposed into wave fields of a two-mode step-gradient index waveguide:

$$E_M(x) = \sum_{l=0}^{1} c_l \cdot \phi_l(x) \quad \text{with} \quad c_l = \int_{-\infty}^{+\infty} \phi_{grd}^*(x) \cdot \phi_l(x) dx\,, \tag{2}$$

where $E_M(x)$ is the field distribution at the input of the two-mode section, $\phi_l(x)$ are the wave functions of the two-mode section of an order l with propagation constants β_l and c_l being the excitation coefficients, defined by overlap integrals. $\phi_{grd}^*(x)$ denotes the conjugated wave function.

The field at the distance z is a superposition of both modal fields with different phase shifts:

$$E_M(x,z) = c_0 \cdot \phi_0(x) \cdot e^{j\beta_0 \cdot z} + c_1 \cdot \phi_1(x) \cdot e^{j\beta_1 \cdot z}\,. \tag{3}$$

In the next propagation step, the field from the end of the two-mode section excites the output gradient-index waveguide. The field at the output of the analyzed structure E_{out} can be expressed by:

$$E_{out}(x,z) = c_{out} \cdot \phi_{grd}(x) \cdot e^{j\beta_{grd} \cdot z}\,, \tag{4}$$

where β_{grd} is the propagation constant and c_{out} is the excitation coefficient of gradient-index waveguide mode.

Taking into account Eqs. (2)–(4), the output power $P(l)$ can be easily determined:

$$P(\lambda) = \left| \int_{-\infty}^{+\infty} \phi_{grd}(x) \cdot \sum_{l=0}^{1} c_l \cdot \phi_l^*(x) \cdot e^{-j\beta_l \cdot L} dx \right|^2, \tag{5}$$

where L is the length of step-index layer. As can be seen, $P(\lambda)$ depends on overlap integrals $\phi_{grd}(x)$ and $\phi_l(x)$ wave functions. Their distributions together with the refractive index distribution of the multimode section is shown in Fig. 3. The calculations were performed for TE polarization.

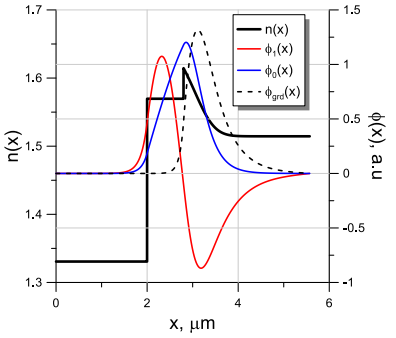

Fig. 3. Refractive index distribution $n(x)$ of multimode section, wave function $\phi_{grd}(x)$ of gradient-index single-mode waveguide and wave functions $\phi_l(x)$ of multimode section at l=0.65mm; diffusion depth d_D=1.1mm and layer thickness w=0.8 mm.

Interference phenomena observed in the examined two-mode waveguide result from the modal properties in the assumed spectral range of the broadband source.

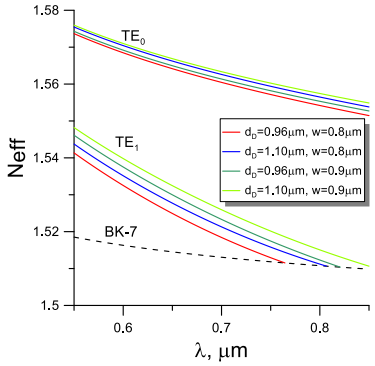

Fig. 4. The dependence of the effective refractive index of modes on the wavelength for the different values of the diffusion depth d_D and the step index layer thickness w.

In Figure 4 effective refractive indices dependences on the wavelengths for the different configurations of the gradient-step index multimode waveguide are presented. It can be seen that the multimode waveguides are two-mode within the assumed values of diffusion depth and step-index layer thickness except for the structure d_D=0.96mm and w=0.8mmm, which is two-mode for the wavelength range 0.55-0.75μm. Figure 5a shows typical spectral characteristics of the output power $P(l)$. The gradient-step index structure of the diffusion depth d_D=1.1mm and the step-index layer thickness w=0.8mm is covered by a water and a water solution with Δn_c=0.005. The characteristics observed are in a close connection with the propagation constants difference Δβ of modes. Their dependence on wavelength in the analysed spectral range is shown in Fig. 5b.

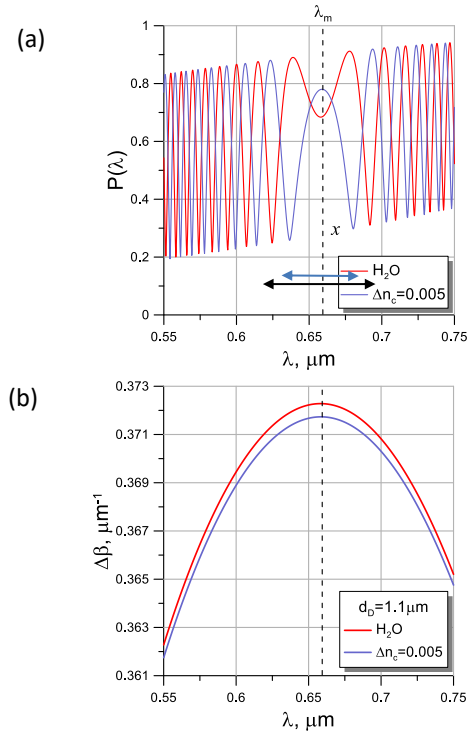

Fig. 5 (a) Spectral characteristics of normalized output power. (b) Propagation constants difference of modes as a function of wavelength.

Characteristic effects occur near the wavelengths close to the value λ_m , which is the maximum of the $\Delta\beta(\lambda)$ function. In that region, propagation constants difference, and in connection with it, the signal's phase changes very slowly with the wavelength. This maximum characteristic value does not depend on the refractive index of the cover.

Spectral characteristics shift is observed with refractive index changes, which is the strongest in the vicinity of λ_m. The signal extremes shift towards longer waves with an increase in the refractive index of the cover for the waves of shorter wavelengths on the left side from the λ_m. On the other hand, the signal extremes shift towards shorter waves with an increase in the refractive index of the cover for the longer wavelengths on the right side from the λ_m. Considering this feature, it is possible to construct one of the possible operating characteristics of the sensor by measuring the mutual shifts x of extremes on both sides of λ_m for different values of the refractive index of the cover (Fig. 5a). On this basis, the sensitivity of the structure can be defined as $S = dx/dn_c$ [μm].

Figures 6 a–b shows the optical structure response for the two different step-index layer thicknesses w. The sensitivity S amounts to 4.65 mm for w=0.8mm, and it reduces to 3.8 mm for w=0.9mm. The step-index layer thickness changes the position of the λ_m and the output spectral distribution. This property makes it possible to fit the optimal waveguide geometry to the input source spectral range. Similar effects have been observed in the case of broadband step-index two-mode interferometers [6] and polarimetric interferometers [7].

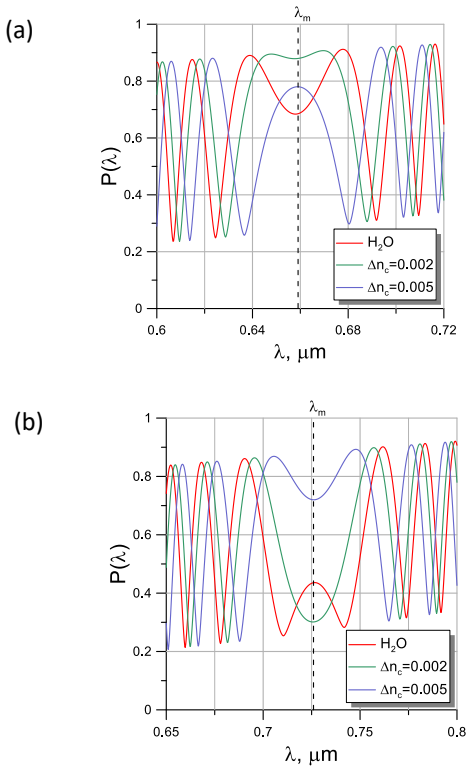

Fig. 6. Spectral characteristics of normalized output power for the different values of refractive index of the cover for the diffusion depth d_D=1.1mm and the step-index layer thickness w equal a) 0.8mm and b) 0.9mm.

The proposed configuration allows refractive index changes to be determined according to the shifts in the spectral distribution of the output signal, rather than measurements of output power changes. For this reason, the method is independent from the input excitation level.

References

[1] M. Błahut, Opt. Appl. **50**, 377 (2020).
[2] M. Nordstrom *et al*., J. Light. Technol. **25**, 1284 (2007).
[3] K. Gut, Nanomaterials **9**, 729 (2019).
[4] M. Błahut, Opt. Appl. **27**, 3 (1998).
[5] https://www.filmetrics.com/refractive-index-database/BK7/Float-Glass
[6] M. Błahut, Phot. Lett. Poland **12**, 28 (2020).
[7] K. Gut, Opt. Expr. **25**, 31111 (2017).

